Molecular Dynamics Simulations of the NGF-TrkA Domain 5 Complex and Comparison with Biological Data

Giovanni Settanni,* Antonino Cattaneo,* and Paolo Carloni*†
*International School for Advanced Studies (SISSA/ISAS); and †National Institute for the Physics of Matter-DEMOCRITOS Modeling Center for Research in Atomistic Simulation, 34014 Trieste, Italy

ABSTRACT The nerve growth factor (NGF) is an important pharmacological target for Alzheimer's and other neurodegenerative diseases. Its action derives partly from its binding to the tyrosine kinase A receptor (TrkA). Here we study energetics and dynamics of the NGF-TrkA complex by carrying out multinanosecond molecular dynamics simulations, accompanied by electrostatic calculations based on the Poisson-Boltzmann equation. Our calculations, which are based on the x-ray structure of the complex, suggest that some of the mutations affecting dramatically the affinity of the complex involve residues that form highly favorable, direct or water-mediated hydrogen bond interactions at the ligand-receptor interface and, in some cases, that also critically participate to the large-scale motions of the complex. Furthermore, our calculations offer a rationale for the small effect on binding affinity observed upon specific mutations involving large changes in electrostatics (i.e., the charged-to-neutral mutations). Finally, these calculations, used along with the mutagenesis data, provide a basis for designing new peptides that mimic NGF in TrkA binding function.

INTRODUCTION

The nerve growth factor (NGF) is a neurotrophin protein dimer essential for the development and maintenance of selected neuronal cells (Bothwell, 1995; Ibanez, 1995). NGF is involved in a large variety of processes, from cell differentiation and survival to growth cessation and apoptosis of neurons. In the last decade, NGF has emerged as a potential target for the treatment of neurodegeneration in Alzheimer's diseases (Yuen and Mobley, 1995). In this respect, the recent determination of the structure of NGF complexed with the cell surface receptor tyrosine kinase A (TrkA) (Wiesmann et al., 1999) has represented a fundamental step for rational drug design, as several of the actions of NGF are thought to result from its interaction with this receptor (TrkA) (Bothwell, 1995; Yuen and Mobley, 1995).

Visual inspection of the structure has revealed that specific domains on NGF, such as the N- and C-termini (Ibanez et al., 1992, 1993; Urfer et al., 1994; Kahle et al., 1992; Drinkwater et al., 1993), and the hairpin loops and residues 91–97 play a pivotal role for the binding (Ibanez et al., 1993; Ilag et al., 1994; Kullander and Ebendal, 1994). Furthermore, the structure has also allowed to rationalize the effect of a very large number of site-directed mutagenesis experiments performed on this receptor (Urfer et al., 1998), on its corresponding NGF ligand (McInnes and Sykes, 1997; Ibanez et al., 1991; Kullander and Ebendal, 1994; Ibanez et al., 1993) and on other neurotrophin ligands, such as BDNF and NT-3 (Urfer et al., 1994, 1997), highly homologous to NGF and binding to receptors of the Trk family.

Still, despite the large amount of structure-function data that has been possible to interpret, several activity measurements of TrkA variants appear difficult to be fully rationalized on the basis of the sole structural information (Ibanez, 1995; Urfer et al., 1998; Guo et al., 1996). Indeed, a number of mutations that involve charge neutralization on residues in direct contact at the NGF-TrkA surface, which disrupt strong electrostatic interactions, turn out not to cause loss of bioactivity (Urfer et al., 1998; Guo et al., 1996). Examples include E324A, E331A, and E334A on TrkA, and R103A on NGF (Table 1). In contrast, replacement of a polar residue with a neutral one, which is expected to cause only a small decrease in the interaction energy (such as in T352A and H353A, Table 1), affects dramatically the binding (Urfer et al., 1998).

Understanding the factors governing the molecular recognition between the TrkA receptor and its ligand would be very important not only to rationalize these data, but also to design novel mutants and eventually design powerful peptide NGF mimics (LeSauteur et al., 1996).

Here we address these issues by means of theoretical methods. Molecular dynamics (MD) simulations, complemented by an electrostatic analysis and a structural analysis of direct and water-mediated hydrogen bond interactions, are carried out on the NGF-TrkA complex in aqueous solution.

The calculations help provide a rationale for many of the mutations of Table 1 and they show that highly persistent, water-mediated H-bond interactions at the protein-protein interface are important for binding. Furthermore, they indicate that the conformational flexibility of the region 352–355 of TrkA is important in the large-scale fluctuations of the NGF-TrkA complex. Finally, they show that persistent hydrogen binding and electrostatics interactions between the N-term and the first part of strand A of NGF and AB and EF

Submitted June 24, 2002, and accepted for publication November 19, 2002.

Address reprint requests to Prof. Paolo Carloni, International School for Advanced Studies, via Beirut 2–4, 34100 Trieste, Italy. Tel.: +39-040-3787-407; Fax: +39-040-3787-528; Email: carloni@sissa.it.

Giovanni Settanni's present address is University of Zurich, Institute of Biochemistry, Winterthurerstrasse 190, CH-8057 Zurich, Switzerland.

0006-3495/03/04/2282/11 $2.00

TABLE 1 Experimentally observed effect of selected interfacial point mutations on TrkA (Urfer et al., 1998) and NGF (Guo et al., 1996) on IC_{50}

	TrkA mutant	IC_{50}(mutant)-IC_{50}(TrkA)
Mutations that largely decrease binding	T352A	>100
	H353A	>100
	P302E	>100
	H343A	78 ± 21
	H343E	68 ± 26
Mutations that do not largely affect binding	E324A	2.0 ± 0.3
	E331A	1.3 ± 0.1
	E334A	3.1 ± 0.1
	E339A	6.6 ± 0.5
	R342A	1.4 ± 0.1
	R347A	1.7 ± 0.1
	E295A	0.6 ± 0.1
	NGF mutant	IC_{50}(mutant)-IC_{50}(TrkA)
Mutations that largely decrease binding	F54A	36
	H4D*	>100
Mutations that do not largely affect binding	Y52A	1.1
	F86A	1.6
	R103A	1.4

*Data from Wiesmann and de Vos (2000).

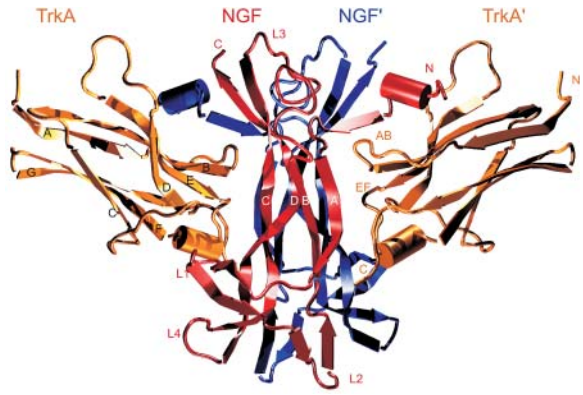

FIGURE 1 Three-dimensional structure of the complex formed by NGF homodimers (*red* and *blue*) and two TrkA domain 5 (*orange*) (Wiesmann et al., 1999). The encoding of the secondary structural elements (which is that used by Wiesmann et al.) and the N- and C-termini are indicated. Two ligand-receptor regions of contact can be identified. The first (*common patch*) comprises the four central β-strands and L1 β-hairpin from NGF and the AB, C′D, and EF loops and C-term from TrkA. The common patch comprises residues well conserved in both the neurotrophin and Trk receptor families (Wiesmann et al., 1999). The second region (*specific patch*, specific for this complex) includes residues from the N-terminus of NGF and from the ABED strand of TrkA.

loop of TrkA play a role in the molecular recognition process along with the long-range electrostatics.

METHODS

Structural model

Our starting model is based on the NGF-TrkA domain 5 complex from *Homo sapiens*, whose x-ray structure has recently been solved at 2.2 Å resolution (Protein Data Bank entry 1www (Wiesmann et al., 1999), Fig. 1). In the structure, NGF subunits are named *V* and *W* and they are numbered from 2 to 115, and 2′ to 115′, respectively; TrkA subunits are named *X* and *Y* and they range from 282 to 382 and from 282′ to 382′. Residues P61(61′), N62(62′), P63(63′), V64(64′), D65(65′), and S66(66′), not present in the x-ray structure, were added using the following procedure: first, the structure of D61(61′), P62(62′), P63(63′),V64(64′), D65(65′), and D66(66′) were extracted from the NGF-serine proteases complex from mouse (Protein Data Bank entry: 1sgf (Bax et al., 1997)). Then, D61(61′), P62(62′), and D66(66′) side chains were replaced by P, P, N, N, D, and D, side chains, respectively, using the Insight II molecular graphics program (Molecular Simulations, San Diego, CA). Finally, the peptide segments were inserted in the NGF structure.

As hydrogen atoms are not detected in the x-ray structure, all His rings were considered as protonated in N_ε on the basis of their putative H-bond interactions. Acetyl and *N*-methyl groups were added at the N-termini and the C-termini of each chain. The overall charge of the complex turned out to be −2. Electroneutrality was insured by adding 2 Na^+ ions, located to D60(D60′) carboxy. The system was immersed in a periodic box of 111 Å × 82 Å × 50 Å containing 13,025 water molecules. The minimum distance between images in neighboring cells was 16 Å.

MD simulations

The all-atom AMBER5 (Pearlman et al., 1995; Cornell et al., 1995; Case et al., 1997) force field was used for the protein and Na^+. The TIP3P model was used for water (Jorgensen et al., 1983).

Periodic boundary conditions were applied. Long-range electrostatic interactions were computed using the particle mesh Ewald method (Darden et al., 1993). A residue-based cutoff of 10 Å was used for the short-range electrostatics and van der Waals interactions. The dielectric constant was set to 1.0. Bonds involving hydrogen atoms were constrained with the SHAKE algorithm (Ryckaert et al., 1977). The time step was set to 1.5 fs. Constant room temperature and pressure simulations were achieved by coupling the systems with a Berendsen thermostat and barostat with 0.2 ps coupling time constant (Berendsen et al., 1984).

The protocol adopted for the simulation was the following: i), minimization of protein hydrogen atoms, sodium counterions, and water molecules; ii), 3 ps MD at room temperature of the same atoms; iii), minimization of the same atoms plus residues 61–66 and 61′–66′; iv), 24 ps MD at room temperature of the same atoms; v) 15 ps MD from 0 K to 300 K at 1 atm pressure of the entire system; and vi), 2.6 ns of MD at room condition (300 K of temperature, 1 atm of pressure). The last 1.9 ns were collected for analysis.

The following properties were calculated:

i. The all-atom root mean-square fluctuation RMSF.
ii. The crystallographic B-factors (Amadei et al., 1993), which were calculated as $B_i = 8\pi^2(RMS_i)^2/3$, where the RMS_i is the RMSF for atom *i* around its average position.
iii. The number of water molecules present in the ligand-receptor interface was calculated by identifying the water oxygens located within 3.5 Å from both receptor and protein ligand.
iv. The number of ordered water molecules at the ligand-receptor interface was calculated as follows: each snapshot of the trajectory was roto-translated so as to keep the protein complex fitted to its initial conformation. Then, a 1 Å cubic grid was defined within the simulation box. The population p_j of each single grid cell *j* was calculated as number of times n_j a water oxygen was present during the dynamics divided by the number *N* of MD steps: $p_j = n_j/N$. The averaged value of p_j turned out to be 0.013(0.009)$Å^{-3}$. The water molecules that occupied the grid cells with MD-average population larger than the value (0.013 + 4 × 0.009) $Å^{-3}$ were defined as ordered water molecules.
v. The H-bond pattern at the interfaces was calculated along the dynamics. H-bonds were detected when the distance between donor and acceptor

heavy atoms was shorter than 4 Å and the angle formed with the hydrogen as vertex was larger than 120°. H-bond interactions at interfaces were divided in three groups: a), direct H-bonds between NGF homodimer and TrkA receptors; b), indirect H-bond interactions between NGF and TrkAs mediated by ordered water, defined as pairs of H-bonds involving a water molecule bridging an atom of the ligand and an atom of the receptor; and c), indirect H-bond interactions between NGF and TrkAs mediated by nonordered interface water. The interactions present for more than half of the simulated time were defined as persistent interactions (Tables 3 and 4, Fig. 6).

Large-scale motions

A principal component (or "essential dynamics") analysis has been performed on the covariance matrix of the C_α's (except those belonging to the residues of chain terminus). The covariance matrix reads: $C_{ij} = \langle (x_i - \langle x_i \rangle) \cdot (x_i - \langle x_i \rangle) \rangle$, where x_i's are the coordinates of the C_α atoms (index $I = 3n$ represents the x coordinate of the n–th C_α, index $I = 3n + 1$ the y coordinate, and index $I = 3n + 2$ the z coordinate). The diagonalization of the covariance matrix, obtained through the SSYEV routine from the LAPACK package (Anderson et al., 1999), led to the identification of the eigenvectors with the largest eigenvalues. Our analysis is limited to the largest eigenvalue, which accounts as much as a third of the total fluctuations. The large-scale motions identified with essential dynamics analysis illustrate cooperative movements of groups of amino acids. These motions can be described as rotations of amino acid domains with respect to other domains according to defined hinge axes (Wriggers and Schulten, 1997). The program Hingefind was used to identify those domains of motions and the hinge axes (Wriggers and Schulten, 1997). Two structures have been provided to the program; the two conformations have been extracted in correspondence of the minimal and maximal projection of the trajectory along the first eigenvector. Only the component parallel to the first eigenvector is kept. Then, the program has divided the amino acids of the complex in optimal domains (the tolerance parameter has been set below the total root mean-square deviation (RMSD) for the pair of structures) (Wriggers and Schulten, 1997), and has identified the hinges of rotation between the domains.

Electrostatics

Two methodologies are here used to identify the interactions that mostly contribute to the electrostatic free energy of binding.

Residue contributions to electrostatic free energy were calculated by solving the Poisson-Boltzmann (PB) equation through the DelPHi (Gilson and Honig, 1988) program. The calculations have been performed on 61 structures extracted from the trajectory of the whole complex every 0.3 ns. Three different calculations were performed for the free components of the complex (TrkA, TrkA′, and NGF homodimer). Water molecules were removed from all the PB calculations. The contributions to the overall electrostatic free energy of binding related to each single amino acid R have been computed as:

$$\Delta G_{\text{bind}}(R) = \frac{1}{2} \sum_{i \in R} q_i (V_i^{\text{comp}} - V_i^{\text{free}}),$$

where q_i is the charge of atom i, and V_i^{comp}, V_i^{free} is the electrostatic potential on the atom i in the complex and in the free components, respectively. For these calculations we used a relative dielectric constant of 78.5 and of 2 for the solvent and the solute, respectively. Ionic strength was set to 0. We have used a cubic grid of 251 points per edge. The PB equation was solved first using a cell size of 4.5Å (10% filling) and Debye-Huckel boundary conditions, followed by a refinement focusing using 0.45 Å cell size (90% filling). Position and dimension of the grid have been kept the same for the PB calculation of the whole complex and its free components to remove the grid self-energy contributions.

The relative relevance of *water-mediated residue-residue interactions* was estimated using the persistency of these interactions. This analysis, although highly approximate, has been validated by comparisons with free-energy data (see Discussion) and therefore it complements the information derived from standard PB approaches, which do not take into account the molecular nature of water.

RESULTS

In this section, we present our findings from a 2.6-ns MD simulation of the NGF-TrkA complex in aqueous solution. The naming convention for the components of the complex has been defined in Methods.

Structural properties

The overall structure of the complex and of the single subunits appear to be equilibrated after ≈0.7 ns, as shown by a plot of the RMS deviations from the energy-minimized structures of the single chains and of the whole complex (Fig. 2 *A*). The average RMSD of TrkA and NGF subunits, calculated over the last 1.9 ns, are 1.5 Å and 2.0 Å, respectively, underlining the larger flexibility of the ligand relative to that of the receptor. Consistently, the distances between NGF and TrkA centers of mass oscillate around an equilibrium conformation after 0.7 ns (Fig. 2 *B*). The secondary structure elements are well conserved during the dynamics, as showed by a comparison between x-ray and MD-averaged structures (Fig. 2 *C*). The final MD conformation exhibits a good Ramachandran plot (Laskowski et al., 1993), except for few residues belonging to loops regions of NGF far from the NGF-TrkA interface (Asp 66, Asp 66′, Asn 46, and Asn 46′), which exhibited φ and ψ angles in relatively high-energy regions.

The structural diversity of the symmetry-related subunits, present in the x-ray structure (Wiesmann et al., 1999) is maintained during the dynamics. The largest discrepancies involve charged groups present in the loops (Table 2 and Fig. 2 *D*), namely: i), the L4 loops, in which Asp 93 interacts with Arg 100 in one subunit and with Lys 34 in the other; ii), the N-term of NGF, in which Arg 9 residue interacts with Glu 334 backbone only in one subunits; and iii), the DE loop, in which Arg 342 interacts toward Glu 339 and Thr 348 carboxyl oxygen in one subunit whereas it interacts with Phe 332 ring in the other.

The TrkA subunits turn out to be much more mobile in our simulation of the complex in water solution than in the crystalline phase: the B-factors calculated along the MD trajectory are larger than those derived by x-ray data (Fig. 3). This difference in mobility and in RMSD (Fig. 1) presumably arises from the absence of packing forces on passing from the crystalline phase, where the TrkA subunits are in close contact with the molecules in neighboring cells, to the aqueous solution.

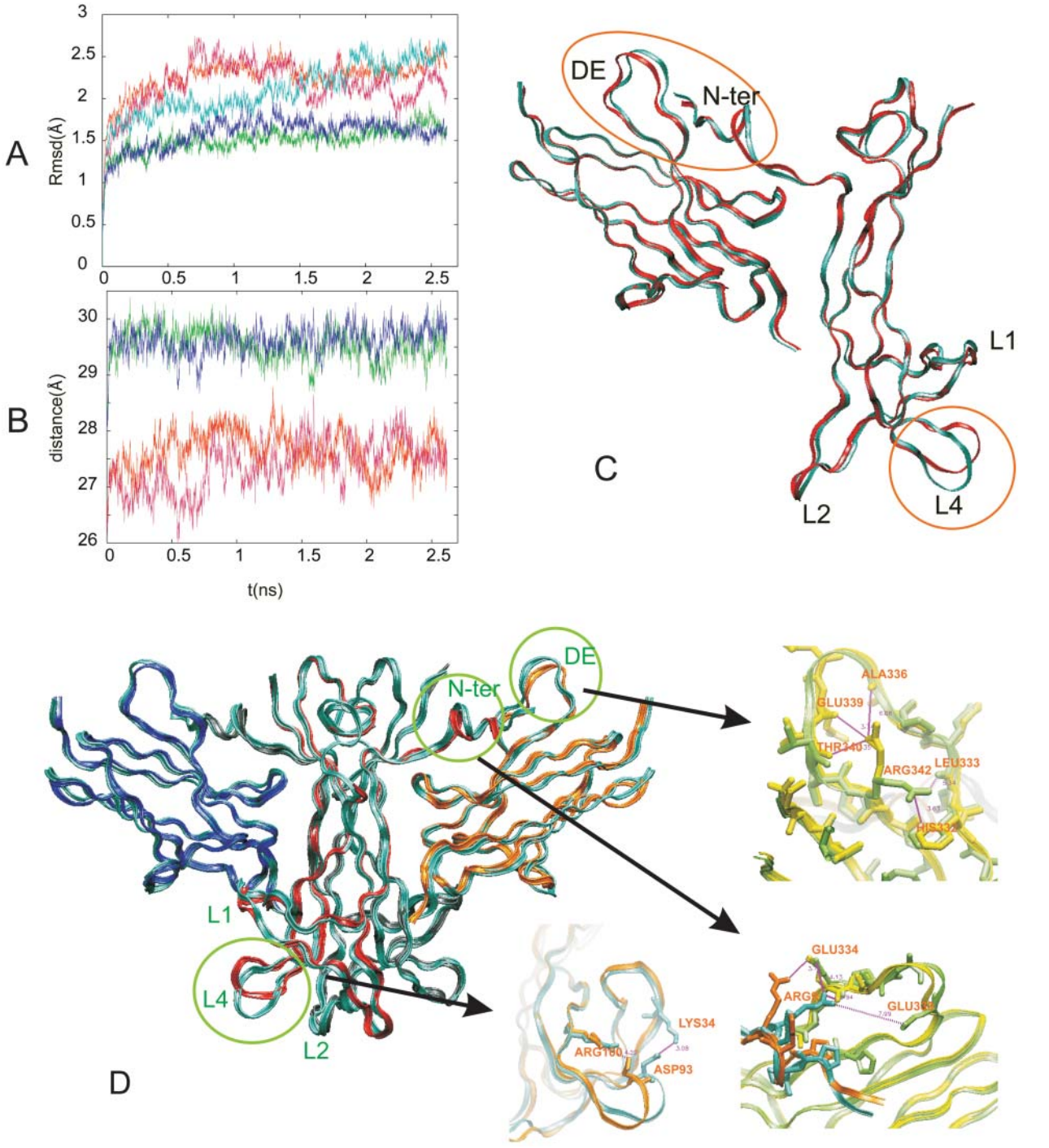

FIGURE 2 MD of NGF-TrkA complex. (*A*) RMSDs from the initial conformation of the entire complex (*red line*), of the TrkA subunits (*blue line*), of NGF (*magenta line*), and NGF′ (*cyan line*). (*B*) Distances between the centers of mass between TrkA and NGF (*red line*), TrkA′ and NGF (*green line*), TrkA and NGF′ (*blue line*), and TrkA′ and NGF′ (*orange line*). (*C*) Comparison between x-ray (*red*) and MD-averaged (*cyan*) structures. Only the backbone of one NGF and one TrkA subunit is shown. (*D*) Comparison between the NGF-TrkA′ (*red*) and the NGF′-TrkA (*cyan*) MD-averaged structures. Only the backbone is shown. Regions exhibiting large discrepancies (*green circles*) are shown at the atomic level (TrkA′, NGF, TrkA, and NGF′ are shown in *green*, *dark green*, *yellow*, and *dark yellow*, respectively).

The residue-residue contacts involved in ligand-receptor interactions are well conserved during the dynamics (the final MD structure is available at http://www.sissa.it/sbp/bc).

The ligand-receptor interfaces are highly hydrated. As many as 55 ± 4(56 ± 5) water molecules are present at the interface between TrkA(TrkA′) and NGF homodimer. Of these water molecules, 20 ± 3(17 ± 3) occupy well-defined and conserved positions during the entire dynamics (ordered

TABLE 2 Selected distances between residues of the complex in the MD-average and in the x-ray structures (see Fig. 2 *D*)

Pairs of atoms	MD-average distance (Å)	X-ray distances (Å)
ARG 342 CZ-PHE 332 Cγ	4.1	4.2
ARG 342′ CZ-PHE 332′ Cγ	9.1	4.4
ARG 342 CZ-THR 340 O	7.3	6.9
ARG 342′ CZ-THR 340′ O	4.0	7.6
ARG 342 CZ-LEU 333 O	5.9	6.7
ARG 342′ CZ-LEU 333′ O	7.3	3.6
ASP 93 Cγ-ARG 100 CZ	5.1	6.5
ASP 93′ Cγ-ARG 100′ CZ	6.7	7.2
ASP 93 Cγ-LYS 34 NZ	8.7	4.9
ASP 93′ Cγ-LYS 34′ NZ	3.5	4.0
ARG 9 CZ-GLU 334′ CD	4.7	7.8
ARG 9′ CZ-GLU 334 CD	5.5	6.6
ARG 9 CZ-GLU 334′ O	7.1	6.0
ARG 9′ CZ-GLU 334 O	4.7	3.7

water molecules, see Methods for definition). Most of these water molecules were already detected in the x-ray structure as highly ordered water molecules (Wiesmann et al., 1999).

Both direct and water-mediated H-bond interactions were detected at the interfaces between ligand and receptor subunits along the trajectory (Table 3). 11 ± 3 (8 ± 2) ordered water molecules and 9 ± 3(9 ± 3) nonordered interface water molecules have been mediating H-bond interactions, on average along the trajectory at the TrkA (TrkA′)-NGF homodimer interfaces. No relevant drift was detected in their numbers. At least 10 direct H-bond interactions per interface turned out to be persistent, i.e., they were present for more than half of the total simulation time (Table 3). Only four of the persistent water-mediated interactions are present at both interfaces, connecting symmetric atoms (Table 4). The persistent H-bond interactions are located in several regions of the TrkA(TrkA′)-NGF homodimer interface (Fig. 6):

1. A large cluster of direct H-bond interactions is located between the EF loop of TrkA(TrkA′) and the strands A, B, C, and D of NGF′(NGF). This cluster connects residues Asn 349(349′) and Gln 350(350′) of TrkA(TrkA′) to residues Arg 103(103′) and His 84(84′) on the NGF homodimer. These direct H-bonds are accompanied by ordered water-mediated interactions involving these residues (except Gln 350), as well as Ser 19′(19) of NGF, Thr 106′, His 84, THR 82, Arg 103 (solely at the TrkA-NGF interface), and Thr 83′ (solely at the TrkA′-NGF′ interface).
2. A cluster of direct H-bond interactions is located between the N-terminus of NGF′(NGF) and B and E strands of TrkA(TrkA′). It involves residues Phe 303(303′) and Gly 344(344′) from TrkA(TrkA′) and residues His 4′(4) from NGF homodimer.
3. A cluster of direct H-bond interactions is located between EF loop of TrkA(TrkA′) and strand A of NGF′(NGF) and involves Trp 21(21′) and His 353′(353). It is accompanied to water-mediated interactions involving Thr 352′(352) and Ile 31(31′) on both interfaces.
4. A cluster of direct H-bond interactions is located between AB loop and F strand of TrKA(TrKA′) and N-term of NGF. It involves residues His 297(297′) and Arg 347(347′) on TrkA(TrkA′), and Glu 11′(11) on NGF′(NGF). It is accompanied by water-mediated interactions involving all of these residues except Arg 347(347′).

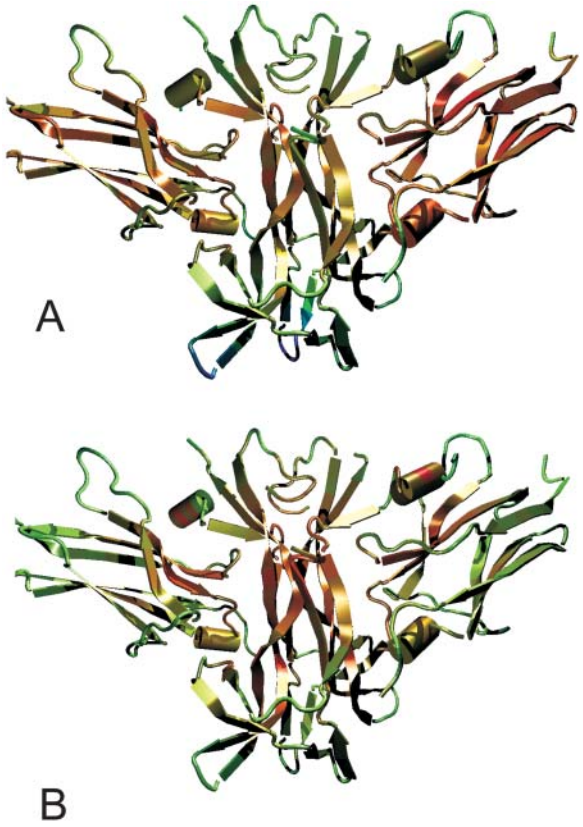

FIGURE 3 Comparison between x-ray derived B-factors (*A*) and those calculated on the basis of the MD simulation (*B*). The most flexible regions are depicted in green, the most rigid in red. As the color scale is normalized to the range of B-factors, it is different in the two cases.

Electrostatics

The electrostatic contribution to the overall free energy of formation of the complex (ΔG_{bind}), here estimated by using the PB equation (Gilson and Honig, 1988), is −116 ± 14 kcal/mol. This high value is expected to be smaller if one uses a nonzero ionic strength in the PB calculations (See Methods).

This stabilizing contribution may arise from both long-range interactions between the NGF and TrkA, and local interactions between residues directly interacting at the ligand-receptor interface. Here we provide a description of these contributions.

TABLE 3 Direct and water-mediated indirect hydrogen bond interactions at the ligand-receptor interfaces

	TrkA-NGF homodimer interface	TrkA′-NGF homodimer interface
Direct hydrogen bond	12.2 ± 1.5 (10)	12.3 ± 1.8 (10)
Indirect interactions mediated by ordered water	24 ± 7 (11)	17 ± 5 (7)
Indirect interactions mediated by nonordered water	19 ± 7 (3)	16 ± 7 (1)

Averages and standard deviations are computed along the equilibrated part of the MD trajectory (See Methods). The number of persistent interactions is reported in parentheses. See Methods for the definitions adopted.

Long-range electrostatic interactions between the subunits highly stabilize the adduct: each TrkA subunit is negatively charged (−4) and each NGF is positively charged (+3). Our calculations show that ligand and receptor are further stabilized by a dipolar coupling (Fig. 4 *A*). Notably, the NGF homodimer is stabilized by dipole-dipole interactions, whereas charge-charge interactions between the two subunits are unfavorable. The global dipolar interactions are fully maintained during the dynamics as the complex is conformationally very stable (see above section).

Short-range electrostatics also plays a role. The electrostatic potentials on the contact surface of ligand and receptor, calculated with the PB equation, are clearly complementary (Fig. 4 *B*): the NGF surface of contact with TrkA is mostly positively charged, with a negative potential region around Glu 11(11′). The TrkA surface of contact with NGF is mostly negatively charged, except for a positive potential region located around Arg 347(347′). These Arg and Glu residues form salt bridges in the x-ray structure, which are maintained during the dynamics (Table 4). The two residues involved in these salt bridges provide highly favorable contributions to the electrostatic free energy of binding ΔG_{bind} (Fig. 4 *C*). Notice that Glu 11(11′) forms persistent H-bonds also to His 297(297′) and His 298(298′) (Table 4).

Other two pairs of salt bridges are present at the ligand-receptor interface. One pair involves Glu 295(295′) from TrKA(TrkA′) and Arg 59′(59) from NGF′(NGF), which form direct H-bonds (Table 4). The other pair involves Glu 334(334′) of TrkA(TrkA′) and Arg 9′(9) of NGF(NGF′), which do not form persistent direct H-bonds (in particular, the Glu 334-Arg 9′ salt bridge is mediated by a water molecule in more than half of the trajectory, Table 4). The residues involved in these interactions provide highly negative contributions to ΔG_{bind} with very large fluctuations along the trajectory (Fig. 4 *C*), in agreement with their relatively lower persistency (Table 4).

Other contributions involving charged residues are those of Glu 331(331′), Glu 324(324′), Glu 339(339′), Arg 342(342′) of TrkA, and Arg 103(103′) of NGF(NGF′). The contributions of the first eight residues show large fluctuations (Fig. 4 *C*), and they are not involved in

TABLE 4 Persistent hydrogen bond interactions at the ligand-receptor interface

	Pair of atoms (TrkAs, NGF)	% of conservation during the dynamics
TrkA-NGF homodimer interface—direct interactions	GLN 350 Oε1-HIS 84 N	100
	ARG 347 NH2-GLU 11′ Oε1	100
	ARG 347 NH1-GLU 11′ Oε1	100
	GLN 350 Nε2-HIS 84 O	98
	ASN 349 O-ARG 103 NH2	96
	ASN 349 Oδ1-ARG 103 NH1	92
	HIS 353 N δ1-TRP 21′ Nε1	90
	GLU 295 Oε2-ARG 59′ NH2	90
	PHE 303 O-HIS 4′ Nε2	87
	GLU 295 Oε2-ARG 59′ NH1	87
	HIS 297 N-GLU 11′ O	81
	ASN 349 O-ARG 103 NH1	81
	GLU 295 Oε1-ARG 59′ NH2	80
	GLU 295 Oε1-ARG 59′ NH1	80
	GLN 350 O-ARG 103 NH2	62
	GLY 344 O-HIS 4′ Nε2	56
TrkA′-NGF homodimer interface—direct interactions	GLN 350′ Oε1-HIS 84′ N	100
	GLN 350′ Nε2-HIS 84′ O	100
	PHE 303′ O-HIS 4 Nε2	98
	ASN 349′ O-ARG 103′ NH2	98
	ARG 347′ NH1-GLU 11 Oε2	98
	ARG 347′ NH2-GLU 11 Oε2	98
	ASN 349′ Oδ1-ARG 103′ NH1	96
	GLU 295′ Oε2-ARG 59 NH2	96
	GLU 295′ Oε1-ARG 59 NH1	96
	GLU 295′ Oε2-ARG 59 NH1	90
	GLY 344′ O-HIS 4 Nε2	85
	HIS 353′ Nδ1-TRP 21 Nε1	83
	GLU 295′ Oε1-ARG 59 NH2	75
	ASN 349′ O-ARG 103′ NH1	71
	HIS 297′ N-GLU 11 O	69
	GLN 350′ O-ARG 103′ NH2	56
TrkA-NGF homodimer interface—indirect interactions mediated by ordered water molecules	ASN 355 Oδ1-ILE 31 O	92
	THR 352 Oγ1-ILE 31 O	90
	HIS 298 N-GLU 11′ O	90
	HIS 297 N-GLU 11′ O	81
	HIS 297 Nδ1-CYS 110 O	77
	GLN 350 Nε2-THR 106′ O	73
	GLN 350 Nε2-HIS 84 O	73
	THR 352 N-ILE 31 O	71
	ASN 349 Nδ2-THR 82 O	69
	GLN 350 O-ARG 103 NH2	52
	GLN 350 Nε2-SER 19′ Oγ	52
TrkA′-NGF homodimer interface—indirect interactions mediated by ordered water molecules	HIS 298′ N-GLU 11 O	94
	GLN 350′ Oε1-THR 83′ Oγ1	73
	THR 352′ Oγ1-ILE 31′ O	58
	THR 352′ Oγ1-LYS 32′ O	52
	HIS 298′ N-GLU 11 Oε2	52
	HIS 297′ N-GLU 11 O	52
	GLN 350′ Nε2-SER 19 Oγ	52
TrkA-NGF homodimer interface—indirect interactions mediated by non-ordered water	GLU 295 Oε2-ARG 59′ NH2	62
	ARG 347 NH1-GLU 11′ Oε2	60
	ARG 347 NH2-TYR 79 OH	52
TrkA′-NGF homodimer interface—indirect interactions mediated by nonordered water	GLU 334′ Oε2-ARG 9 NH1	52

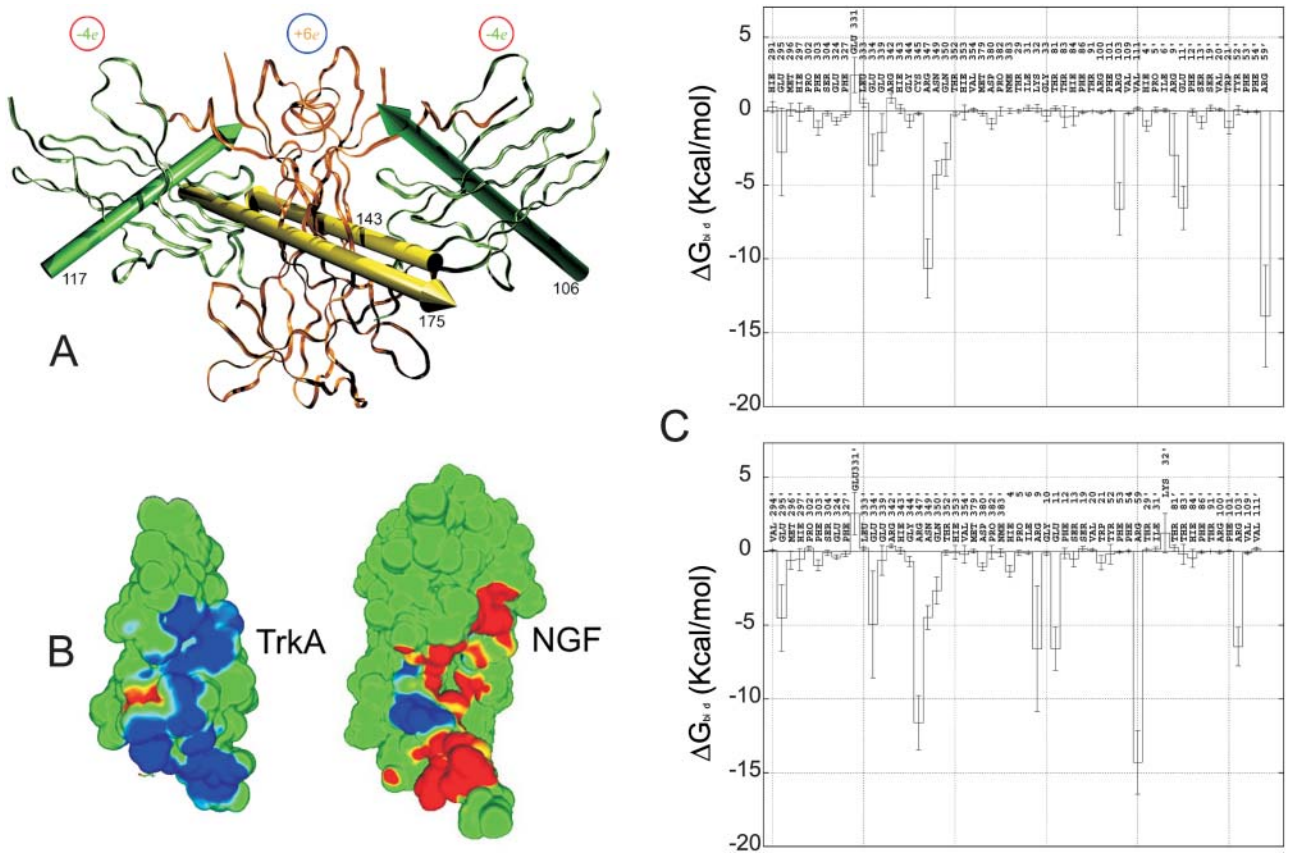

FIGURE 4 Ligand-receptor electrostatic interactions. (*A*) Stabilizing long-range interactions are provided by the opposite charges on the receptor (*green*) and ligand (*yellow*) (in atomic units). The calculated gas phase values of the dipoles are reported. The effective values of the dipoles are expected to be much smaller because of the screening of the protein complex. (*B* and *C*) Electrostatic potential and potential energy obtained by solving the Poisson-Boltzmann equation (Gilson and Honig, 1988). Calculations are carried out on 61 equally spaced conformations from the trajectory and the results are averaged. (*B*) Electrostatic potential on the NGF and TrkA van der Waals surfaces involved in the formation of the complex. Blue and red represent regions of negative and positive potential, respectively. (*C*) Electrostatic free energies of binding (ΔG_{bind}) of residues at the NGF-TrkA (*upper graph*) and NGF-TrkA′ (*lower graph*) interfaces. *Left*: Residues belonging to the receptor; *right*: residues belonging to the ligand.

persistent H-bond interactions. We further notice that the contribution of Glu 331(331′) is positive. The contribution of Arg 103(103′) is large and exhibits small fluctuations (Fig. 4 *C*), presumably because of their persistent H-bond interactions with Asn 349(349′) and, to a smaller extent, to Gln 350(350′) of TrkA(TrkA′) (Table 4).

Also other few interactions are present that involve noncharged residue(s) providing stabilizing electrostatic binding free energy (Fig. 4 *C*): i), His 4′ (4) from NGF (NGF′), which form persistent H-bonds both with Phe 303 (303′) and (to a lesser extent) with Gly 344(344′) backbone oxygen atoms from TrkA(TrkA′) (Table 4); and ii), Trp 21(21′) from NGF, which form a persistent H-bond to His 353′ (353) Nδ1 from TrkA′(TrkA) (Table 4).

Water-mediated H-bonds

Here we use our structural analysis of H-bond pattern to detect the persistency of these interactions. Our analysis shows that Thr 352(352′), Ile 31(31′), Lys 32(32′), and Thr 83(83′) form only water-mediated interactions (Table 4), and do not show relevant contributions to the electrostatic free energy (Fig. 4 *C*). Furthermore, several residues that form direct H-bond interactions also form water-mediated H-bonds: His 297 (297′)-Glu 11′(11), Gln 350(350′)-His 84(84′), Glu 295-Arg 59′, and Arg 347-Glu 11′ (Table 4).

Large-scale motions

The long time fluctuations can be probed as eigenvectors associated to the covariance matrix of the C_α atoms (Amadei et al., 1993). Within our timescale, the largest collective motion, associated to the largest eigenvector of the covariance matrix, involves a rotation of the TrkA subunits around the NGF homodimer (Fig. 5 *A*). A projection of the components of the motion onto the C_α shows that the largest components are localized on TrkA and TrkA′ domains and on the N- and C-termini of NGF and NGF′. The latter strictly follow the motion of the TrkA subunits (Fig. 5 *B*). A plot of the distribution of the conformations as a function of their

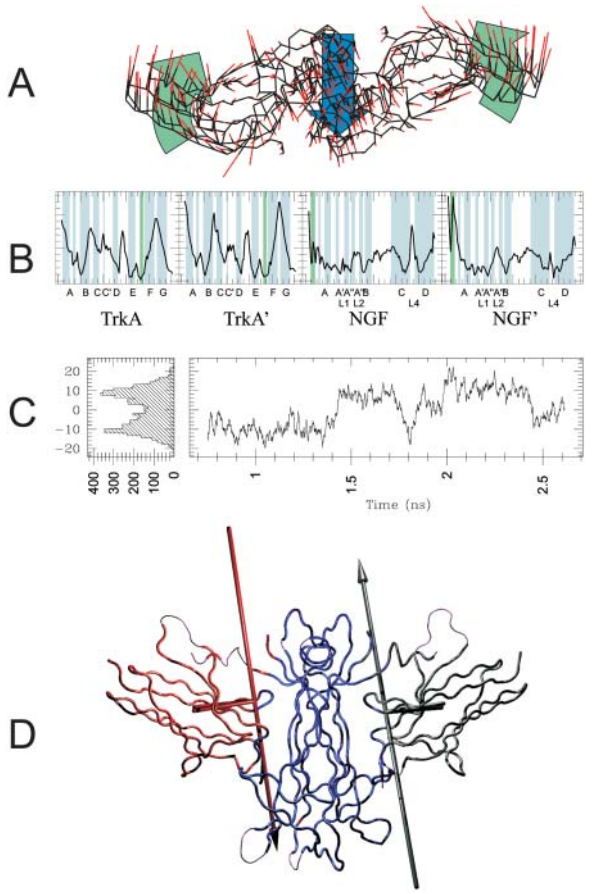

FIGURE 5 Large-scale motions of the complex. Several properties of the largest eigenvector of the covariance matrix are represented. (*A*) The eigenvector is represented as a vector field on the C_α atoms of the MD-averaged structure. The red-ended stick departing from every C_α atom is proportional (both in length and direction) to the component of the eigenvector along that atom. Large arrows (*blue*, NGF; *green*, TrkA) pictorially represent the sum of the motion of the amino acids of each domain. (*B*) The moduli of the components represented in (*A*) are plotted as function of the C_α atoms. β-strand and α-helix conformations are depicted in blue and green, respectively. The labels on the *x* axis indicate the secondary structure elements and the loops of NGF (Wiesmann et al., 1999). (*C*) *Right*: Projection of the trajectory along the eigenvector as a function of time. The nonmonotonic behavior indicates a good sampling of the conformational space and the absence of slow drifts in the simulation. *Left*: Distribution of the projection. The presence of a double peak suggests the existence of two well-separated ensembles of conformations. (*D*) According to the analysis of Wriggers and Schulten (1997), this large-scale motion can be visualized as a rotation of the TrkA subunits (in *red* and *gray*) around the hinge axis of the complex (also in *gray* and *red*).

projection on this eigenvector (Fig. 5 *C*) suggests that the motion samples two distinct ensembles of conformations. Analysis of the conformations carried on with the program Hingefind (Wriggers and Schulten, 1997) indicates that the main difference consists in the rotation of the TrkA subunits (relative to NGF) around the hinge axis of the complex (Fig. 5 *D*). The angular difference between the two positions is 10° for both TrkA subunits. The residues lying close to the hinge axis are mostly involved in the motion because of their action as a fulcrum for the rotation. They comprise residues 297–299, 336–339, 348, and 350–355 on both TrKA and TrkA′; and residues 3–11, 46, 93–96, and 112–114 on both NGF and NGF′. Interestingly, some of these residues also show relevant interfacial electrostatic or hydrogen bond interactions (Fig. 6).

DISCUSSION

We have investigated structural, energetic and dynamical aspects of the NGF-TrkA complex in aqueous solution by theoretical methods.

Our MD-averaged structural properties of NGF-TrkA complex in aqueous solution are similar to those emerging from the x-ray structure (Wiesmann et al., 1999). As expected, however, the TrkA subunits are more mobile than in the crystalline phase, where the TrkA subunits are in close contact with the molecules in neighboring cells (Figs. 1 *A* and 2).

The structural differences between NGF-TrkA and NGF-TrkA′ interfaces, already detected in the x-ray structure, are fully maintained (Fig. 2).

Our electrostatic analysis suggests that long- and short-range electrostatic interactions provide significant contributions to the overall affinity of the complex. Long-range electrostatics, such as charge-charge, charge-dipole, and dipole-dipole TrkA-NGF interactions, stabilizes the complex (Fig. 4 *A*). Furthermore, the shape of the electrostatic potential, calculated with the PB equation (Gilson and Honig, 1988) at the surfaces of contact between ligand and receptor is complementary, and provides highly stabilizing direct H-bonding and salt bridge interactions (Fig. 4 *B*).

In addition, our calculations suggest that the ligand-receptor surface is highly hydrated by the presence of ≈20 ordered water molecules and 35 nonordered water molecules. We found that, on average, more than 30 pairs of atoms are linked at each interface by bridging water molecules. Only a fraction of these water-mediated interactions are nonpersistent (i.e., they are only present in a small fraction of the trajectory, Table 3). On the other hand, ordered water molecules mediate interactions between the surface of the ligand and the receptor.

An accurate estimate of the energetics associated to these water-mediated H-bond interactions cannot be obtained using standard PB approaches, which consider implicitly the presence of the solvent. Attempts have been made to explicitly consider mediating water molecules in PB calculations (see, e.g., Langen et al., 1992; Yang et al., 1993; Fitch et al., 2002). Here we attempt to use an alternative approach to these electrostatic analyses by estimating the strength of water-mediated H-bonds based on our structural analysis. To validate this approach, comparison is first made between the persistency of direct H-bond interactions and the contributions of these interactions to the

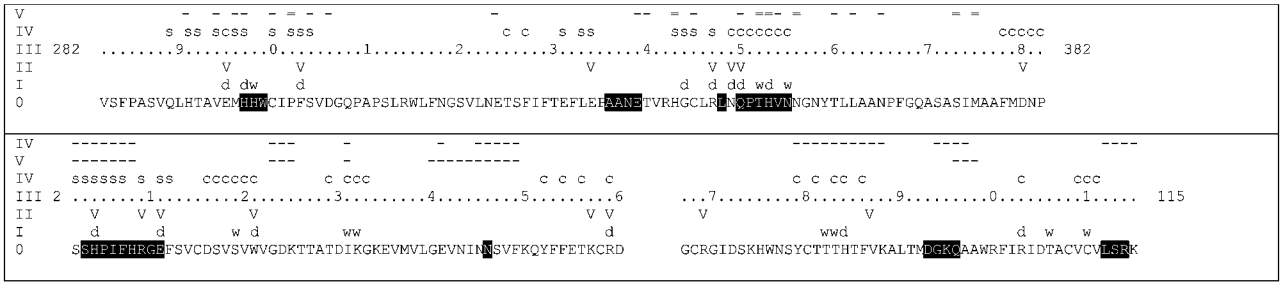

FIGURE 6 Selected biological and calculated properties of TrkA (*top*) and of NGF (*bottom*). (*Top*) (*0*) Primary sequences. Residues within 5 Å from the hinge axes in the MD-averaged structure have been marked with black background. This set comprises residues from the N- and C-terminus of NGF homodimer, from L1 and L4 loops of NGF and from the AB and EF loops of TrkA. (*I*) Residues involved in direct (*d*) or water-mediated indirect (*w*) hydrogen bond interactions with residues on the opposite surface. (*II*) Residues characterized by markedly favorable (*V*) electrostatic free energies (ΔG_{bind} in Fig. 4 *C*). (*III*) Residues numbering according to Wiesmann et al. (1999). (*IV*) Residues belonging to the specific (*s*) or to the common patch (*c*) of TrkA, as defined in Wiesmann et al. (1999). (*V*) Residues whose mutations are known that affect slightly (-) or largely (=, $IC_{50} > 100$) the binding constant (Urfer et al., 1998). (*Bottom*) (*I–IV*) Same as *A*. (*V–VI*) The residues whose mutations are known to increase (*V*) or to disrupt the biological function (*VI*) of NGF are marked with "-" (Ibanez, 1995).

total electrostatic free energy of binding. Table 4 shows that the direct H-bonds exhibiting high persistency mainly take place between the N-terminus of NGF′(NGF) and AB loop of TrKA(TrkA′) and the interactions between strand A of NGF(NGF′) and EF loop of TrkA′(TrkA), and involve His 4(4′), Glu11(11′), Trp 21(21′), Arg 59(59′), and Arg 103(103′) of NGF, and Glu 295(295′), Phe 303(303′), Arg 347(347′), Asn 349(349′), and Gln 350(350′). These residues also provide large electrostatic free-energy contributions (Figs. 4 *C* and 6). Based on the correlation between persistency and free-energy data, we now use our structural analysis to provide a qualitative estimation of the relative strength of persistent, water-mediated H-bond interactions. Our approach suggests therefore that residues Glu 295, His 297(297′), His 298(298′), Arg 347, Asn 349, Gln 350(350′), Thr 352(352′), Asn 355 on TrkAs and Arg 9, Glu 11, Ser 19(19′), Ile 31(31′), Lys 32′, Arg 59′, Thr 82, Thr 83′, His 84, Tyr 79, Arg 103, and Thr 106′ on NGF (Table 4) are expected to provide significant contributions to the affinity of the complex as they form persistent, water-mediated, H-bond interactions. Thus, based on our analysis, the binding affinity in this complex is not only achieved through direct protein-protein interactions, but also by exploiting the water molecules located at the interface, which act as a sort of glue between ligand and receptor.

Finally, our calculations provide information on the large-scale motions of the complex. They suggest that the complex undergoes a well-defined motion on the nanosecond time scales, involving an oscillation of the TrkAs around the NGF homodimer (Fig. 5). The motion occurs as a coordinated rotation of the TrkA subunits around the NGF homodimer (Fig. 5 *A*). The rotation involves residues of the NGF homodimer, (particularly from N-terminus and from L1 and L4 loop) and of TrkA (residues from 348 to 355, Fig. 6). The latter also form persistent direct and water-mediated H-bond interactions, which might provide the contact surface flexibility that is needed for this motion to occur.

Comparison with biological data

In this section, we use our calculations to interpret some of the mutagenesis data by (Urfer et al., 1998) and (Guo et al., 1996) presented in Table 1. Because of the simplicity of the analysis used here, we focus only on residues forming electrostatic and/or H-bonding interactions.

Explanations for the large effects on the affinity upon mutating polar residues into neutral or charged residues may be offered based on our simulation-analysis. His 4(4′) and His 353(353′) side chains form direct H-bond interactions with Phe 303′(303) and Trp 21′(21), respectively. These interactions are highly persistent (Table 4) and, accordingly, residues His 4(4′) Phe 303(303′), and Trp 21(21′) provide highly stabilizing electrostatic free energy of binding (Figs. 4 *C* and 6). Thus, the mutations of His 4(4′) and His 353(353′) in Asp and Ala, respectively (Table 1), may cause the disruption of such stabilizing interactions, which in turn could be a key factor for the experimentally observed large decrease in binding activity of NGF (Wiesmann and de Vos, 2001). In addition, the introduction of a net charge in the His-4-Asp mutant could also affect the binding. The side chain of residues Thr 352(352′) form water-mediated, highly persistent H-bond interactions with Ile 31(31′) (Table 4). Thus, their mutation to Ala could disrupt the H-bond interactions, causing the decrease in binding affinity experimentally observed (Table 1). Finally, the mutations involving Pro 302 and His 343 on TrkA (Table 1) may affect the persistent direct H-bonds formed by the backbone atoms of Phe 303(303′) and Gly 344(344′) (Table 4), which in turn may alter the binding affinity, as experimentally observed.

The mutation of His 353(353′) and Thr 352(352′) might also affect the molecular recognition by altering the mechanical properties of the complex. Indeed, because of the proximity of these residues to the hinge axes (Fig. 6), their mutation might affect the large-scale motions of the protein, which in turn might be important for the function of the

complex (Wriggers and Schulten, 1998). That is, the flexibility of the H-bond network formed by these residues might be an important ingredient for the motion to occur and their mutation may eventually lead to an impairment of the function of the complex.

The small effect on the binding affinity observed upon charged to neutral mutations (except for Glu 11(11′), Arg 347(347′), and Arg 103(103′)) (Table 1) may be interpreted, at least in part, in terms of their electrostatic free energies of binding calculated with the PB equation. Indeed, the latter are relatively small and/or exhibit large fluctuations (Fig. 4 *C*), suggesting that the destabilization due to the mutations might be small with respect to the large stabilizing contributions deriving from long-range electrostatics as well as from hydrophobic interactions or water-mediated interactions (see above). In addition, this mutation-induced destabilization may also be smaller than the large stabilizing contributions from electrostatics interactions of Arg 347(347′) on TrkA, and Arg 103(103′) and Glu 11(11′) on NGF; thus, it may not be sufficient to significantly affect the binding affinity of the complex. On the other hand, the simulation-analysis we performed do not allow to explain the small effect on binding affinity upon mutation of Arg 347(347′) and Arg 103(103′); this limitation of our approach may be due to a structural relaxation of the complex upon mutation; this process is neglected in our calculations that are based on the wild-type complex and it could be described by simulations of the mutated system.

The nonpolar solvation contributions are not included in our calculations. Thus, the effect of mutations of the NGF-TrkA complex involving aromatic residues Tyr 52 and Phe 86 (Table 1), which form hydrophobic interactions (Wiesmann and de Vos, 2001), and are not involved in H-bonding interactions, cannot be rationalized based on our simple analysis. Also, our simple analysis does not take into account the van der Waals and the internal energy and the entropic contributions due to conformational changes and loss of mobility of the bound proteins (Srinivasan et al., 1998; Kuhn and Kollman, 2000). Indeed, it is well known that PB electrostatic free energy of binding of ligand-receptor complexes may also result positive (i.e., unfavorable to binding) (Sheinerman and Honig, 2002), indicating that, in such cases, complex stabilization comes from the other mentioned contributions. Finally, our estimate of the relative strength of water-mediated interactions is rather approximate, as it is based on structural data. Nevertheless, we show here that our simple simulation-analysis provides a qualitative explanation for most of the data presented in Table 1. Quantitative estimations require more sophisticated approaches, such as MD-based free-energy calculations.

Implications for the design of a peptide mimic

Our calculations, along with mutagenesis data, allow for drawing a feasible strategy for the design of NGF mimetic peptides. Indeed, our results suggest that the NGF residues His 4, Glu 11, and Trp 21 in the specific patch (Figs. 4 *C* and 6) and in the first part of strand A of NGF provide highly persistent H-bond interactions to the complex (Figs. 4 *C* and 6) along with large favorable electrostatic free-energy contributions. This is consistent with mutagenesis data, which show that mutations on residues belonging to this part of the complex (such as His 4 on NGF, and Met 296, His 297, and Gln 350 on TrkA) largely affect its affinity (Table 1, Fig. 6, and references therein). Besides these favorable electrostatic interactions, the hydrophobic interactions between residues Ile 6 and Phe 7 from NGF and Val 294, Met 296, Pro 302, and Leu 333 (Wiesmann and deVos, 2001) stabilize even more the binding of the N-term of NGF to TrkA. On the other hand, these residues are not conserved along the neurotrophin family or Trk receptor family (Wiesmann and de Vos, 2001); thus they provide particular specificity for the NGF-TrkA binding. A peptide consisting of the N-terminal part of NGF is expected to have high affinity for the receptor. Furthermore, it is expected to be highly specific for this complex, as the N-term NGF-TrkA interactions are not present in other neurotrophin-receptor systems (Wiesmann et al., 1999).

CONCLUSIONS

Our calculations help clarify the functional role of some amino acids playing a crucial part in NGF-TrkA binding (Table 1, Fig. 6), not emerging from visual inspection of the x-ray structure of the NGF-TrkA complex. This work has also provided the basis for the design of new peptides that mimic NGF in TrkA binding function. These should exploit the interactions present at the specific patch and between the beginning of NGF strand A and AB loop of TrkA that involve both hydrophobic burial, hydrogen bonding, and electrostatics. Work is in progress in our laboratory to test these proposals.

REFERENCES

Amadei, A., A. B. Linssen, and H. J. Berendsen. 1993. Essential dynamics of proteins. *Proteins*. 17:412–425.

Anderson, E., Z. Bai, C. Bischof, S. Blackford, J. Demmel, J. Dongarra, J. Du Croz, A. Greenbaum, S Hammarling, A. McKenney, and D. Sorensen. 1999. LAPACK Users' Guide. Society for Industrial and Applied Mathematics. Philadelphia, PA.

Bax, B., T. L. Blundell, J. Murray-Rust, and N. Q. McDonald. 1997. Structure of mouse 7S NGF: a complex of nerve growth factor with four binding proteins. *Structure*. 5:1275–1285.

Berendsen, H. J., J. P. M. Postma, W. F. van Gunsteren, A. Di Nola, and J. R. Haak. 1984. Molecular dynamics with coupling to an external bath. *J. Chem. Phys*. 81:3684–3690.

Bothwell, M. 1995. Functional interactions of neurotrophins and neurotrophin receptors. *Annu. Rev. Neurosci*. 18:223–253.

Case, D. A., D. A. Pearlman, J. W. Caldwell, T. E. Cheatham III, W. S. Ross, C. L. Simmerling, T. A. Darden, K. M. Merz, R. V. Stanton, A. L. Cheng, J. J. Vincent, M. Crowley, D. M. Ferguson, R. J. Radmer, G. L.

Seibel, U. C. Singh, P. K. Weiner, and P. A. Kollman. 1997. AMBER 5. UCSF, San Francisco. http://www.amber.ucsf.edu/amber/amber.html.

Cornell, W. D., P. Cieplak, C. I. Bayly, I. R. Gould, K. M. Merz, D. M. Ferguson, D. C. Spellmeyer, T. Fox, J. W. Caldwell, and P. A. Kollman. 1995. A 2nd generation force-field for the simulation of proteins, nucleic-acids, and organic-molecules. *J. Am. Chem. Soc.* 117:5179–5197.

Darden, T., D. York, and L. Pedersen. 1993. Particle mesh Ewald: an N.log(N) method for Ewald sums in large systems. *J. Chem. Phys.* 98:10089–10092.

Drinkwater, C. C., P. A. Barker, U. Suter, and E. M. Shooter. 1993. The carboxyl-terminus of nerve growth-factor is required for biological-activity. *J. Biol. Chem.* 268:23202–23207.

Fitch, C. A., D. A. Karp, K. K. Lee, W. E. Stites, E. E. Lattman, and B. Garcia-Moreno. 2002. Experimental pK_a values of buried residues: analysis with continuum methods and role of water penetration. *Biophys. J.* 82:3289–3304.

Gilson, M. K., and B. Honig. 1988. Calculations of the total electrostatic energy of a macromolecular system: solvation energies, binding energies, and conformational analysis. *Proteins.* 4:7–18.

Guo, M., S. L. Meyer, H. Kaur, J. Gao, and K. Neet. 1996. Mutational studies of conserved residues in the dimer interface of nerve growth factor. *Protein Sci.* 5:447–455.

Ibanez, C. F. 1995. Neurotrophic factors: from structure-function studies to designing effective therapeutics. *Trends Biotechnol.* 13:217–227.

Ibanez, C. F., T. Ebendal, G. Barbany, J. Murray-Rust, T. L. Blundell, and H. Persson. 1992. Disruption of the low affinity receptor-binding site in NGF allows neuronal survival and differentiation by binding to the Trk gene product. *Cell.* 69:329–341.

Ibanez, C. F., T. Ebendal, and H. Persson. 1991. Chimeric molecules with multiple neurotrophic activities reveal structural elements determining the specificities of NGF and BDNF. *EMBO J.* 10:2105–2110.

Ibanez, C. F., L. L. Ilag, J. Murray-Rust, and H. Persson. 1993. An extended surface of binding to Trk tyrosine kinase receptors in NGF and BDNF allows the engineering of a multifunctional pan-neurotrophin. *EMBO J.* 12:2281–2293.

Ilag, L. L., P. Lonnerberg, H. Persson, and C. F. Ibanez. 1994. Role of variable beta-hairpin loop in determining biological specificities in neurotrophin family. *J. Biol. Chem.* 269:19941–19946.

Jorgensen, W. L., J. Chandrasekhar, and J. D. Madura. 1983. Comparison of simple potential functions for simulating liquid water. *J. Chem. Phys.* 79:926–935.

Kahle, P., L. E. Burton, C. H. Schmelzer, and C. Hertel. 1992. The amino terminus of nerve growth factor is involved in the interaction with the receptor tyrosine kinase p140trkA. *J. Biol. Chem.* 267: 22707–22710.

Kuhn, B., and P. A. Kollman. 2000. Binding of a diverse set of ligands to avidin and streptavidin: an accurate quantitative prediction of their relative affinities by a combination of molecular mechanics and continuum solvent model. *J. Med. Chem.* 43:3786–3791.

Kullander, K., and T. Ebendal. 1994. Neurotrophin-3 acquires NGF-like activity after exchange to five NGF amino acid residues: molecular analysis of the sites in NGF mediating the specific interaction with the NGF high affinity receptor. *J. Neurosci. Res.* 39:195–210.

Langen, R., G. M. Jensen, U. Jacob, P. O. Stephens, and A. Warshel. 1992. Protein control of iron-sulfur cluster redox potentials. *J. Biol. Chem.* 267:25625–25627.

Laskowski, R. A., M. W. MacArthur, D. S. Moss, and J. M. Thornton. 1993. Main-chain bond lengths and bond angles in protein structures. *J. Appl. Crystallogr.* 26:283–291.

LeSauteur, L., N. K. V. Cheung, R. Lisbona, and H. U. Saragovi. 1996. Small molecule nerve growth factor analogs image receptors in vivo. *Nat. Biotechnol.* 14:1120–1122.

McInnes, C., and B. D. Sykes. 1997. Growth factor receptors: structure, mechanism, and drug discovery. *Biopolymers.* 43:339–366.

Pearlman, D. A., D. A. Case, J. W. Caldwell, W. S. Ross, T. E. Cheatham, S. Debolt, D. Ferguson, G. Seibel, and P. Kollman. 1995. Amber, a package of computer-programs for applying molecular mechanics, normal-mode analysis, molecular-dynamics and free-energy calculations to simulate the structural and energetic properties of molecules. *Comput. Phys. Commun.* 91:1–41.

Ryckaert, J. P., G. Ciccotti, and H. J. C. Berendsen. 1977. Numerical integration of the Cartesian equations of motion of a system with constraints: molecular dynamics of n-alkanes. *J. Comp. Phys.* 23: 327–341.

Sheinerman F. B. and B. Honig. 2002. On the role of electrostatic interactions in the design of protein-protein interfaces. *J. Mol. Biol.* 318:161–177.

Srinivasan, J., T. E. Cheatham, P. Cieplak, P. A. Kollman, and D. A. Case. 1998. Continuum solvent studies of the stability of DNA, RNA and phosphoramidate-DNA helices. *J. Am. Chem. Soc.* 120:9401–9409.

Urfer, R., P. Tsoulfas, L. O'Connell, J. A. Hongo, W. Zhao, and L. G. Presta. 1998. High resolution mapping of the binding site of TrkA for nerve growth factor and TrkC for neurotrophin-3 on the second immunoglobulin-like domain of the Trk receptors. *J. Biol. Chem.* 273:5829–5840.

Urfer, R., P. Tsoulfas, L. O'Connell, and L. G. Presta. 1997. Specificity determinants in neurotrophin-3 and design of nerve growth factor-based TrkC agonists by changing central beta-strand bundle residues to their neurotrophin-3 analogs. *Biochemistry.* 36:4775–4781.

Urfer, R., P. Tsoulfas, D. Soppet, E. Escandon, L. F. Parada, and L. G. Presta. 1994. The binding epitopes of neurotrophin-3 to its receptors TrkC and Gp75 and the design of a multifunctional human neurotrophin. *EMBO J.* 13:5896–5909.

Wiesmann, C., and A. M. de Vos. 2001. Nerve growth factor: structure and function. *Cell. Mol. Life Sci.* 58:748–759.

Wiesmann, C., M. H. Ultsch, S. H. Bass, and A. M. de Vos. 1999. Crystal structure of nerve growth factor in complex with the ligand- binding domain of the TrkA receptor. *Nature.* 401:184–188.

Wriggers, W., and K. Schulten. 1997. Protein domain movements: detection of rigid domains and visualization of hinges in comparisons of atomic coordinates. *Proteins.* 29:1–14.

Wriggers, W., and K. Schulten. 1998. Nucleotide-dependent movements of the kinesin motor domain predicted by simulated annealing. *Biophys. J.* 75:646–661.

Yang, A. S., M. R. Gunner, R. Sampogna, K. Sharp, and B. Honig. 1993. On the calculation of pKas in proteins. *Proteins.* 15:252–265.

Yuen, E. C., and W. C. Mobley. 1995. Therapeutic applications of neurotrophic factors in disorders of motor-neurons and peripheral-nerves. *Mol. Med. Today.* 1:278–286.